AGU PUBLICATIONS

JGR

Journal of Geophysical Research: Space Physics

RESEARCH ARTICLE

10.1002/2013JA019397

Special Section:
The Causes and Consequences of the Extended Solar Minimum between Solar Cycles 23 and 24

Coronal electron temperature in the protracted solar minimum, the cycle 24 mini maximum, and over centuries

N. A. Schwadron[1,2], M. L. Goelzer[1], C. W. Smith[1], J. C. Kasper[3], K. Korreck[3], R. J. Leamon[4], S. T. Lepri[5], B. A. Maruca[6], D. McComas[2,7], and M. L. Steven[3]

[1]University of New Hampshire, Durham, New Hampshire, USA, [2]Southwest Research Institute, San Antonio, Texas, USA, [3]Harvard-Smithsonian Center for Astrophysics, Cambridge, Massachusetts, USA, [4]Department of Physics, Montana State University, Bozeman, Montana, USA [5]Department of Atmospheric, Oceanic and Space Sciences, University of Michigan, Ann Arbor, Michigan, USA [6]Space Sciences Laboratory, University of California,Berkeley, California, USA, [7]Also at University of Texas at San Antonio, San Antonio, Texas, USA

Key Points:
- Corona abnormally cool during mini maximum
- Cycle 24 similar to Dalton Minimum
- Solar wind scaling law validated by cycle 24 data

Correspondence to:
N. A. Schwadron,
n.schwadron@unh.edu

Citation:
Schwadron, N. A., M. L. Goelzer, C. W. Smith, J. C. Kasper, K. Korreck, R. J. Leamon, S. T. Lepri, B. A. Maruca, D. McComas, and M. L. Steven (2014), Coronal electron temperature in the protracted solar minimum, the cycle 24 mini maximum, and over centuries, *J. Geophys. Res. Space Physics*, *119*, 1486–1492, doi:10.1002/2013JA019397.

Received 4 SEP 2013
Accepted 1 FEB 2014
Accepted article online 12 FEB 2014
Published online 26 MAR 2014

Abstract Recent in situ observations of the solar wind show that charge states (e.g., the O^{7+}/O^{6+} and C^{6+}/C^{5+} abundance ratios) evolved through the extended, deep solar minimum between solar cycles 23 and 24 (i.e., from 2006 to 2009) reflecting cooler electron temperatures in the corona. We extend previous analyses to study the evolution of the coronal electron temperature through the protracted solar minimum and observe not only the reduction in coronal temperature in the cycles 23–24 solar minimum but also a small increase in coronal temperature associated with increasing activity during the "mini maximum" in cycle 24. We use a new model of the interplanetary magnetic flux since 1749 to estimate coronal electron temperatures over more than two centuries. The reduction in coronal electron temperature in the cycles 23–24 protracted solar minimum is similar to reductions observed at the beginning of the Dalton Minimum (~1805–1840). If these trends continue to reflect the evolution of the Dalton Minimum, we will observe further reductions in coronal temperature in the cycles 24–25 solar minimum. Preliminary indications in 2013 do suggest a further post cycle 23 decline in solar activity. Thus, we extend our understanding of coronal electron temperature using the solar wind scaling law and compare recent reductions in coronal electron temperature in the protracted solar minimum to conditions that prevailed in the Dalton Minimum.

1. Introduction

The deep solar minimum between cycles 23 and 24 and the activity in cycle 24 differed significantly from those of the prior cycle [*Schwadron et al.*, 2011; *McComas et al.*, 2013]. In the solar minimum, the fast wind was slightly slower, was significantly less dense and cooler, had lower mass and momentum fluxes [*McComas et al.*, 2008], and weaker heliospheric magnetic fields [*Smith and Balogh*, 2008]. In the rise of activity in cycle 24, the mass flux of solar wind remained low [*McComas et al.*, 2013] and the magnetic flux of the heliosphere remained at significantly lower levels than observed at previous solar maxima in the space age [*Smith et al.*, 2013]. The current "mini" solar maximum of cycle 24 shows only a small recovery in particle and magnetic fluxes [*McComas et al.*, 2013]. Therefore, the cycle 24 mini solar maximum is far more like the protracted solar minimum than previous maxima observed during the space age.

Ulysses observations showed that the charge state ratios O^{7+}/O^{6+} and C^{6+}/C^{5+} and the abundance ratio Fe/O significantly decreased during the cycles 23–24 minimum [*Zhao and Fisk*, 2010]. The charge state ratios O^{7+}/O^{6+} and C^{6+}/C^{5+} are commonly used to infer electron freezing-in temperatures set low in the corona (within $\sim 3R_s$, where R_s is one solar radius) where the solar wind drags ions out more rapidly than ionization and recombination can equilibrate them to the local electron temperature. *Schwadron et al.* [2011] found that (for a given solar wind speed) the coronal electron temperature (as derived from O^{7+}/O^{6+} and C^{6+}/C^{5+} measurements from ACE) decreased during the cycles 23–24 solar minimum.

Kasper et al. [2012] showed that for relatively narrow bins of solar wind speeds (bin widths of 50 km/s), the coronal electron temperature derived from solar wind charge states dropped through the deep cycles 23–24 minimum. The reductions in coronal temperature were associated with significant reductions in the solar wind He abundance. *McIntosh et al.* [2011] found that the (supergranular) network emission length scale varied with that of the helium abundance and the degree of iron fractionation in the solar wind. The decrease

in the helium abundance and the degree of iron fractionation (approaching values of the photosphere) in the fast wind indicated a significant change in the loading of material into the fast solar wind. *Lepri et al.* [2013] also studied solar wind charge states during the deep protracted minimum and concluded that coronal heating was significantly reduced compared to previous minima. The observation of [*Kasper et al.*, 2012] that coronal temperature dropped for a roughly fixed speed of solar wind was pivotal as it clearly showed that some other factor in addition to coronal electron temperature must control the speed of solar wind. According to the solar wind scaling law [*Schwadron and McComas*, 2003], the particle flux also plays a major role in controlling the solar wind speed. The energy-per-particle lost through downward heat flux scales as $T_m^{7/2}/(f_0 L)$ where T_m is the maximum coronal electron temperature at or below a scale height, f_0 is the particle flux near the base of the flux tube, and L is the length along a flux tube to the maximum electron temperature T_m. Therefore, lower particle fluxes near the base of a flux tube cause more significant energy losses from heat flux conduction.

Schwadron et al. [2011] used the solar wind scaling law [*Schwadron and McComas*, 2003] to show that cooler coronal electron temperatures are naturally associated with lower particle fluxes during the protracted minimum [*McComas et al.*, 2008; *Schwadron and McComas*, 2008] because downward heat conduction must be reduced to keep the average energy loss per particle fixed. The results of the scaling law suggested that the evolution of the solar wind is linked to the solar dynamo, which caused the coronal magnetic field strength to decrease in the deep, extended minimum. Further, *Schwadron et al.* [2011] utilized the scaling law to project coronal electron temperatures backward in time throughout the space age and found that these temperatures have been decreasing in successive temperature maxima since 1987, but had been increasing in successive temperature maxima from 1969 to 1987.

The solar wind scaling law [*Schwadron and McComas*, 2003] used by *Schwadron et al.* [2011] relates a solar wind stream's 1 AU speed to coronal electron temperature and the particle flux near its source. The energy budget of any coronal heating model can be understood using the scaling law. Higher coronal electron temperatures at the source of a flux tube may be the result of higher heating rates.

The physical principles on which the *Schwadron and McComas* [2003] scaling law is based are well known: the strong dependence of the solar wind speed on coronal electron temperature is due to coronal heat conduction, which sets pressure in loops [*Rosner et al.*, 1978] and the inner boundary conditions of solar wind [e.g., *Hammer*, 1982; *Leer et al.*, 1982]. In regions where conductive losses are small, the 1 AU wind speed achieves its maximum steady state value $u_{\max}$ of roughly 800 km s^{-1}, $mu_{\max}^2/2 = m\bar{v}_a^2 - GM_s m/R_s$ and the coronal source electron temperature is cool, as observed in coronal holes.

This article extends the analysis of *Schwadron et al.* [2011] in several respects. We are able to explore observations made during the rise of cycle 24 to test whether the prediction holds that the increase of solar wind flux and magnetic flux during increasing activity also cause increased coronal electron temperatures. We will see that these natural predictions of the solar wind scaling law are confirmed by recent charge state observations from the Solar Wind Ion Composition Spectrometer on ACE. Further, we make use of new estimates of magnetic flux since 1749 [*Goelzer et al.*, 2013] to develop estimates of coronal electron temperatures over centuries. This first-time historic reconstruction of coronal electron temperatures allows us to contextualize of recent anomalies observed in coronal and solar wind properties over the protracted cycles 23–24 minimum and the "mini" cycle 24 maximum.

2. Observations and the Solar Wind Scaling Law

A key question in the cycle 24 maximum is how the Sun recovers from the protracted cycles 23–24 minimum. ACE data has been reanalyzed to glean any possible information about increasing coronal temperatures from charge states in cycle 24. Figure 1 shows what is largely a reanalysis of *Schwadron et al.* [2011] including all available charge state data (including data in 2010 and beyond) and a number of additional improvements including removal of coronal mass ejections (CMEs) identified by *Cane and Richardson* [2003], inclusion only of model results with fractional uncertainties less than 25% and observations of flux made for 10 or more consecutive 1 h intervals. In addition, we define tighter 0.75 year time-bins, which are essential for resolving statistically significant increases in coronal temperature associated with activity in cycle 24. As in *Schwadron et al.* [2011], we compare coronal temperatures from charge states (solid lines) to the results of

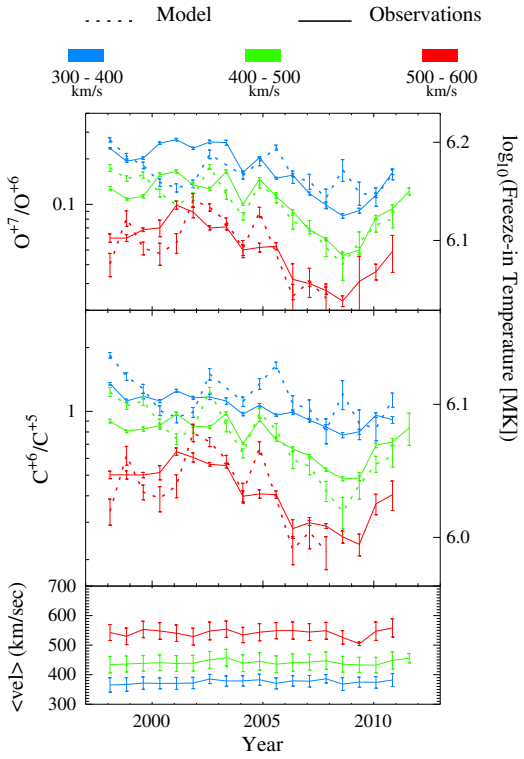

Figure 1. Coronal freezing-in temperature deduced from O^{7+}/O^{6+} and C^{6+}/C^{5+} charge state ratios (solid curves) in the speed bins shown and in 0.75 year time-bins. The analysis used here is similar to *Schwadron et al.* [2011] with key differences being (1) the addition of new data in 2010 and beyond, (2) smaller time-bins to resolve increases in coronal temperatures associated with cycle 24 activity, and (3) the use of the *Cane and Richardson* [2003] CME list to identify and remove anomalous behavior due to CMEs.

the solar wind scaling law (dashed lines). In *Schwadron et al.* [2011], we found the reduction in coronal temperature through to 2009, whereas the current study resolves the increase in coronal temperature in 2010 and 2011 due to increasing solar activity in these years.

As done in *Schwadron et al.* [2011], we quantify the relative root-mean-square (RMS) departures between the model and observations,

$$\Delta = \sqrt{\frac{1}{N}\sum_{i=1}^{N}\frac{(O_i - E_i)^2}{O_i^2}} \quad (1)$$

where O_i represents an observation, and E_i an expectation value for the O^{7+}/O^{6+} or C^{6+}/C^{5+} charge state ratio produced by our model. We calculate the relative RMS departures from the scaling law model and from the mean of observations. Table 1 shows these results. Departures from the scaling law model are generally smaller than the departures from the mean values in each speed bin, particularly for the O^{7+}/O^{6+} ratio. The exception is in the lowest speed bin (300–400 km/s) of the C^{6+}/C^{5+} ratio where the mean value fits the data as well or better than the scaling law model. This departure from the scaling law in the lowest speed solar wind may reflect nonsteady processes (such as opening loops, the injection of material from the tips of the helmet streamer, or other processes involving interchange reconnection to form the slow solar wind).

The key *observational* result that stands out in Figure 1 is that coronal temperatures do increase in the cycle 24 maximum. However, coronal temperatures do not recover to their previous highs in cycle 23. Figure 2 shows extended analysis of the scaling law into cycle 24 using OMNI data. We find not only the increase in coronal temperatures of cycle 24 but also a drop of coronal temperatures in the most recent data. This result suggests not only that we may have already extended through the cycle 24 maximum in 2013, but also that we have begun descent into the cycles 24–25 minimum for the 400–500 and 500–600 km/s speed bins. Coronal temperatures continue to show remarkably low values indicative of the anomalous lack of solar activity in the era that began approximately in 2005.

In recent work, insights into the evolution of the interplanetary magnetic flux [e.g., *Schwadron et al.*, 2010] were used to determine its time history based on sunspot number since 1749 [*Goelzer et al.*, 2013]. The *Schwadron et al.* [2010] theory treats two components of the interplanetary magnetic field: the magnetic

Table 1. RMS Relative Deviations (Δ) of Model (Δ_{model}) and Means of Charge State Ratio (Δ_{mean}) for Each Velocity Bin[a]

Type	300–400 (km/s)	400–500 (km/s)	500–600 (km/s)
Δ_{model} (O^7/O^6, %)	37	24	32
Δ_{mean} (O^7/O^6, %)	47	52	53
$\Delta_{mean}/\Delta_{model}$ **(O^7/O^6)**	**1.3**	**2.2**	**1.6**
Δ_{model} (C^5/C^5, %)	29	23	29
Δ_{mean} (C^6/C^5, %)	16	25	33
$\Delta_{mean}/\Delta_{model}$ **(C^6/C^5)**	**0.6**	**1.1**	**1.2**

[a]Bold text emphasizes the significance of deviations with respect to the mean.

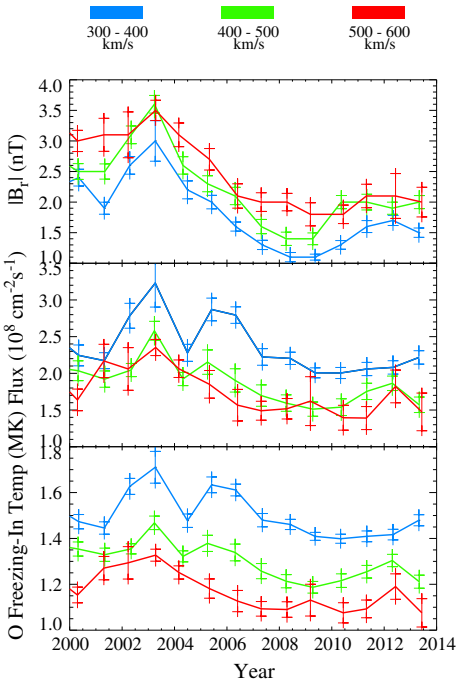

Figure 2. (bottom) Results of the scaling law for O freezing-in temperature derived from the scaling law. The curves shown here are in the same speed bins as Figure 1. In this case, we utilize OMNI data (http://omniweb.gsfc.nasa.gov/) for the (middle) 1 AU particle flux, bin by speed and form 1 year medians and uncertainties. Also shown is the (top) unsigned radial magnetic field strength, which serves as a proxy for the magnetic flux in solar wind.

flux associated with ejecta and the magnetic flux associated with the steady solar wind. *Schwadron et al.* [2010] write the rate of CME-associated flux (Φ_{ej}) as follows:

$$\frac{d\Phi_{ej}}{dt} = f(1-D)\phi_{CME} - \Phi_{ej}\left(\frac{1}{\tau_{ic}} + \frac{1}{\tau_d} + \frac{1}{\tau_o}\right) \quad (2)$$

where f is the rate of CME injection as a function of time, D is the fraction of CME flux reconnected immediately after release, ϕ_{CME} is the flux content of a typical CME, τ_{ic} is the interchange time scale between ejecta-associated flux and open flux, τ_d is the time scale for disconnection and loss of ejecta-associated and open magnetic flux, and τ_o is the time scale for "opening"—the conversion of ejecta-associated into open flux. *Schwadron et al.* [2010] details these time scales further. One additional equation is introduced to account for the rate of change of open magnetic flux:

$$\frac{d\Phi_o}{dt} = -\frac{\Phi_o - \Phi_{flr}}{\tau_d} + \frac{\Phi_{ej}}{\tau_o} \quad (3)$$

where Φ_{flr} allows for a minimum "floor" for the open flux [*Wang et al.*, 2000; *Owens et al.*, 2008; *Zhao et al.*, 2009; *Lockwood et al.*, 2009; *Crooker and Owens*, 2010], which *Goelzer et al.* [2013] sets to zero. Following *Smith et al.* [2013], *Goelzer et al.* [2013] scales the frequency of CME ejection (f) with sunspot number (from the NOAA Geophysical Data Center (NGDC)) and specifies the constants D=1/2, τ_{ic}=20 days, τ_d=6 years. The result is a model of the heliospheric magnetic field strength as a function of time with primary input being the solar sunspot number.

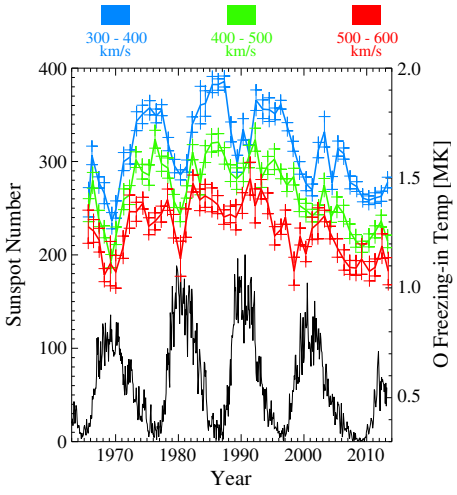

Figure 3. The O freezing-in temperature (red, green, and blue curves) from the solar wind scaling law plotted with monthly sunspot number (black lines) (http://www.sidc.be).

Figure 3 compares estimated freezing-in temperatures and sunspot numbers. Note that the reductions in sunspot number do appear associated with lower freezing-in temperature in 2013. While this again supports the concept that we have begun descent in solar activity, we also see in cycles such as 23 the presence of a double peak in sunspot numbers. Time will tell if we have in fact gone beyond solar maximum in 2013.

The *Goelzer et al.* [2013] time history of magnetic flux is used to estimate solar wind particle flux using the direct scaling between particle and magnetic flux [*Schwadron and McComas*, 2008]: $\dot{M}_{sw}/\Phi_B$=1.25 mg s^{-1} Wb^{-1} where $\dot{M}_{sw}$ solar wind mass loss and Φ_B is the solar wind magnetic flux. With particle flux estimated in this way, we solve for coronal electron temperature (the equivalent of the oxygen freezing-in temperature) since 1749 using the solar wind scaling law (Figure 4, left).

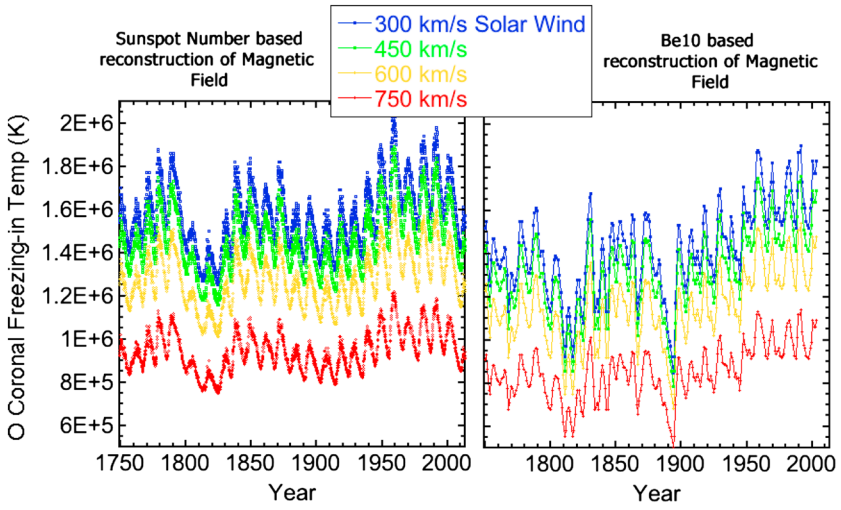

Figure 4. The O freezing-in temperature since 1749 from the solar wind scaling law using solar wind particle flux scaled from interplanetary magnetic field strength. We show both the results when using the magnetic field reconstruction based on (left) sunspot number by *Goelzer et al.* [2013] and (right) reconstruction based on ^{10}Be measurements by *McCracken and Beer* [2007]. The model of the interplanetary magnetic field is derived from a rate balance equation taking into account that the total flux of the interplanetary magnetic field evolves over the solar cycle due to a combination of flux that extends well outside of 1 AU and is associated with the solar wind, and additionally, transient flux associated with coronal mass ejections (CMEs). In addition to the CME eruption rate, there are three fundamental processes involving conversion of magnetic flux (from transient to wind associated), disconnection and interchange reconnection that control the levels of each form of magnetic flux in the interplanetary medium [*Schwadron et al.*, 2010; *Smith et al.*, 2013]. The CME rate is based on the history of sunspot numbers, which allows us to derive the time history of interplanetary magnetic flux over hundreds of years [*Goelzer et al.*, 2013].

There is a wide array of sunspot-based and geomagnetic reconstructions of the heliospheric magnetic field [e.g., *Solanki et al.*, 2000; *Lockwood*, 2013, and references therein]. In principle, the techniques employed here to reconstruct coronal temperatures could be applied using any reconstruction of the heliospheric magnetic field. Therefore, it is informative to consider a second example in which we estimate historic coronal temperatures using a reconstruction of the heliospheric magnetic field based on ^{10}Be, a radionuclide that is deposited into polar ice due to spallation reactions with galactic cosmic rays in the atmosphere and subsequent precipitation. During lower solar activity, enhanced fluxes of galactic cosmic rays produce larger numbers of radionuclides that become trapped in polar ice. Ice core samples are used to determine the level of solar activity down to an ~1 year resolution. Through comparison with sunspot data and recorded heliospheric magnetic field strength, it has been shown that sunspot minima and the corresponding changes to the heliospheric magnetic field correlates with increases in the ^{10}Be levels [*McCracken and Beer*, 2007; *McCracken et al.*, 2013]. These studies depend on the calibration of *Caballero-Lopez et al.* [2004] for ^{10}Be versus heliospheric magnetic field strength. Figure 2 (right) shows the results using the ^{10}Be reconstruction [*McCracken and Beer*, 2007] of the heliospheric magnetic field.

The similarity between the evolution of sunspot numbers in cycles 23 and 24 has allowed *Goelzer et al.* [2013] to estimate how cycle 24 will decline. *Goelzer et al.* [2013] predict the coming 10 years of sunspot numbers by noting that early in 2013 marks the peak in the solar cycle. Prior to this the onset of the Dalton Minimum closely resembles the last 15 years, and at this point the sunspot number is comparable to what was seen during the first reduced maximum of the Dalton Minimum. The years following 1805 thereby serve as a prediction for the coming 10 years of solar activity. With the 10 year predictions of sunspot number, the theory of *Schwadron et al.* [2010] is applied to determine the levels of interplanetary magnetic flux [*Goelzer et al.*, 2013]. The conversion of magnetic flux to particle flux and application of the solar wind scaling law to infer coronal temperature is performed in the same manner as indicated previously. Figure 5 shows the results for coronal electron temperature (oxygen freezing-in temperature) in the years leading up to 2013 and then the resulting prediction for the coming solar minimum computed using the Dalton Minimum years 1805 onward. Specifically, the prediction using this projection of sunspot number is that coronal

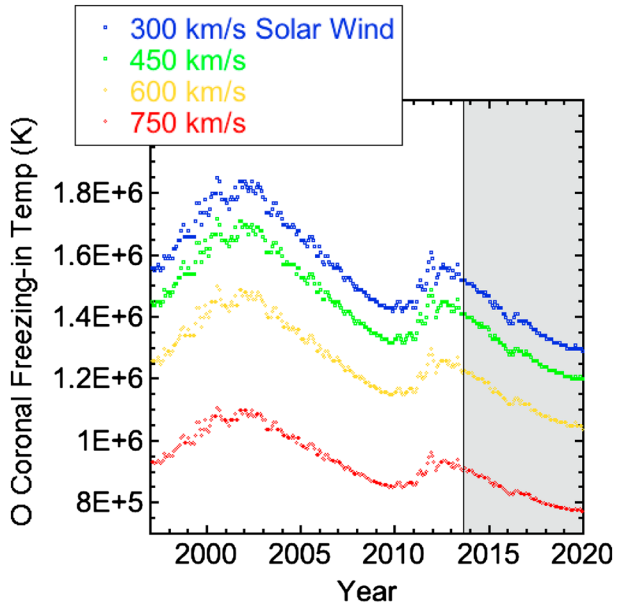

Figure 5. The estimated O freezing-in temperature from 1997 to present and projected out to 2020 (shaded region) from the solar wind scaling law using solar wind particle flux scaled from projections of the interplanetary magnetic field strength [*Goelzer et al.*, 2013]. The model of the interplanetary magnetic field is derived from a rate balance equation [*Schwadron et al.*, 2010; *Smith et al.*, 2013] with CME rate estimated from sunspot numbers [*Goelzer et al.*, 2013]. The projection of sunspot numbers beyond 2013 is estimated from sunspot number evolution during the Dalton Minimum, which showed remarkable similarity to the evolution from cycles 23 to 24.

temperatures will fall to levels even lower than observed in the protracted cycles 23–24 minimum. There are preliminary indications of post cycle 24 decline in solar activity in Figure 2.

3. Summary

We have extended the study of *Schwadron et al.* [2011] by showing that the solar wind scaling law agrees with observations in the deep solar minimum between cycles 23 and 24 and the slight increase in solar activity in the mini maximum of cycle 24. We observe further preliminary indications in 2013 of declining activity following the cycle 24 maximum.

The solar wind scaling law follows from scaling injected Poynting flux and particle flux based on large-scale magnetic flux in the heliosphere. The scaling law takes into account energy losses in the form of heat conduction and gravitational potential. As a result, our model predicts changes in the solar corona based on the evolution of the heliospheric magnetic field. A significant strength of the scaling law is that it applies not only for the evolution of fast and slow wind in previous (normal) solar cycles, but also during the abnormal mini maximum of solar cycle 24. The additional years of analysis extended from *Schwadron et al.* [2011] through the mini maximum therefore provides significantly stronger support for the solar wind scaling law.

The *Goelzer et al.* [2013] model of heliospheric magnetic flux is derived by scaling the rate of coronal mass ejections in proportion to sunspot numbers. This provides the basis to estimate heliospheric magnetic flux since 1749. The solar wind scaling law is applied here to estimate coronal temperatures over hundreds of years. We observe a similar reduction in coronal temperatures during the cycles 23–24 minimum as we find during the period near the beginning of the 1800s at the start of the Dalton Minimum. This suggests that the next solar minimum may continue to show declining coronal temperatures and further reductions in solar wind particle flux.

In summary, we have shown that the evolution of coronal freezing-in temperatures over the solar cycle observed with the ACE spacecraft is consistent with the solar wind scaling law. Reduction in coronal temperatures and particle flux over the cycles 23–24 minimum and their small increase in the mini maximum of cycle 24 are related to the evolution of the heliospheric magnetic field. The projection of the scaling law backward in time since 1749 suggests that the abnormally low coronal temperature and particle flux in the mini maximum of cycle 24 may be similar to conditions that prevailed near the beginning of the Dalton Minimum in the early 1800s.

Acknowledgments

N.A.S. was supported by LRO/CRaTER (NASA contract NNG11PA03C), the NASA Coronal-Solar Wind Energetic Particle Acceleration Modules (C-SWEPA; NASA grant NNX07AC14G) project, the NSF Sun-2-Ice project (NSF grant AGS1135432), the Solar Probe Plus Integrated Investigation of the Sun (SPP-ISIS) project, and the DREAM 2 investigation (NASA Grant NNX10AB17A). Both C.W.S. and M.L.G. were supported by the ACE/MAG Caltech subcontract 44A-1062037 to UNH. D.M.C. was supported by ACE/SWEPAM. J.C.K., M.L.S., K.E.K., and B.A.M. were supported by the WIND/SWE project. K.K. was supported by the NSF-Solar REU program. We thank the ACE SWICS and SWIMS instrument team and the Ion Mass Spectrometer (SWIMS) ACE Science Center for providing the ACE data.

Philippa Browning thanks the reviewers for their assistance in evaluating this paper.

References

Caballero-Lopez, R. A., H. Moraal, K. G. McCracken, and F. B. McDonald (2004), The heliospheric magnetic field from 850 to 2000 AD inferred from ^{10}Be records, *J. Geophys. Res.*, *109*, A12102, doi:10.1029/2004JA010633.

Cane, H. V., and I. G. Richardson (2003), Interplanetary coronal mass ejections in the near-Earth solar wind during 1996–2002, *J. Geophys. Res.*, *108*(A4), 1156, doi:10.1029/2002JA009817.

Crooker, N. U., and M. J. Owens (2010), Impact of coronal mass ejections, interchange reconnection, and disconnection on heliospheric magnetic field strength. ArXiv e-prints.

Goelzer, M. L., C. W. Smith, N. A. Schwadron, and K. G. McCracken (2013), An analysis of heliospheric magnetic field flux based on sunspot number from 1749 to today and prediction for the coming solar minimum, *J. Geophys. Res. Space Physics*, *118*, 7525–7531, doi:10.1002/2013JA019404.

Hammer, R. (1982), Energy balance of stellar coronae - Part two - Effect of coronal heating, *Astrophys. J.*, *259*, 779, doi:10.1086/160214.

Kasper, J. C., M. L. Stevens, K. E. Korreck, B. A. Maruca, K. K. Kiefer, N. A. Schwadron, and S. T. Lepri (2012), Evolution of the relationships between helium abundance, minor ion charge state, and solar wind speed over the solar cycle, *Astrophys. J.*, *745*, 162, doi:10.1088/0004-637X/745/2/162.

Leer, E., T. E. Holzer, and T. Fla (1982), Acceleration of the solar wind, *Space Sci. Rev.*, *33*, 161–200.

Lepri, S. T., E. Landi, and T. H. Zurbuchen (2013), Solar wind heavy ions over solar cycle 23: ACE/SWICS measurements, *Astrophys. J.*, *768*, 94, doi:10.1088/0004-637X/768/1/94.

Lockwood, M. (2013), Reconstruction and prediction of variations in the open solar magnetic flux and interplanetary conditions, *Living Rev. Sol. Phys.*, *10*, 4, doi:10.12942/lrsp-2013-4.

Lockwood, M., M. Owens, and A. P. Rouillard (2009), Excess open solar magentic flux from satellite data: 2. A survey of kinematic effects, *J. Geophys. Res.*, *114*, A11104, doi:10.1029/2009JA014450.

McComas, D. J., R. W. Ebert, H. A. Elliott, B. E. Goldstein, J. T. Gosling, N. A. Schwadron, and R. M. Skoug (2008), Weaker solar wind from the polar coronal holes and the whole Sun, *Geophys. Res. Lett.*, *35*, L18103, doi:10.1029/2008GL034896.

McComas, D. J., N. Angold, H. A. Elliott, G. Livadiotis, N. A. Schwadron, R. M. Skoug, and C. W. Smith (2013), Weakest solar wind of the space age and the current "mini" solar maximum, *Astrophys. J.*, *779*, 2, doi:10.1088/0004-637X/779/1/2.

McCracken, K., J. Beer, F. Steinhilber, and J. Abreu (2013), The heliosphere in time, *Space Sci. Rev.*, *176*, 59–71, doi:10.1007/s11214-011-9851-3.

McCracken, K. G., and J. Beer (2007), Long-term changes in the cosmic ray intensity at Earth, 1428–2005, *J. Geophys. Res.*, *112*, A10101, doi:10.1029/2006JA012117.

McIntosh, S. W., K. K. Kiefer, R. J. Leamon, J. C. Kasper, and M. L. Stevens (2011), Solar cycle variations in the elemental abundance of helium and fractionation of iron in the fast solar wind: Indicators of an evolving energetic release of mass from the lower solar atmosphere, *Astrophys. J.*, *740*, L23, doi:10.1088/2041-8205/740/1/L23.

Owens, M. J., N. U. Crooker, N. A. Schwadron, T. S. Horbury, S. Yashiro, H. Xie, O. C. S. Cyr, and N. Gopalwamy (2008), Conservation of open solar magnetic flux and the floor in the heliospheric magnetic field, *Geophys. Res. Lett.*, *35*, L20108, doi:10.1029/2008GL035813.

Rosner, R., W. H. Tucker, and G. S. Vaiana (1978), Dynamics of the quiescent solar corona, *Astrophys. J.*, *220*, 643.

Schwadron, N. A., and D. J. McComas (2003), Solar wind scaling law, *Astrophys. J.*, *599*, 1395–1403.

Schwadron, N. A., and D. J. McComas (2008), The solar wind power from magnetic flux, *Astrophys. J. Lett.*, *686*, L33–L36, doi:10.1086/592877.

Schwadron, N. A., et al. (2010), Earth-Moon-Mars Radiation Environment Module framework, *Space Weather*, *8*, S00E02, doi:10.1029/2009SW000523.

Schwadron, N. A., et al. (2011), Coronal electron temperature from the solar wind scaling law throughout the space age, *Astrophys. J.*, *739*, 9, doi:10.1088/0004-637X/739/1/9.

Smith, C. W., N. A. Schwadron, and C. E. DeForest (2013), Decline and recovery of the interplanetary magnetic field during the protracted solar minimum, *Astrophys. J.*, *775*, 59, doi:10.1088/0004-637X/775/1/59.

Smith, E. J., and A. Balogh (2008), Decrease in heliospheric magnetic flux in this solar minimum: Recent Ulysses magnetic field observations, *Geophys. Res. Lett.*, *35*, L22103, doi:10.1029/2008GL035345.

Solanki, S. K., M. Schüssler, and M. Fligge (2000), Evolution of the Sun's large-scale magnetic field since the Maunder minimum, *Nature*, *408*, 445–447, doi:10.1038/408445a.

Wang, Y.-M., J. Lean, and N. R. Sheeley Jr. (2000), The long-term variation of the Sun's open magnetic flux, *Geophys. Res. Lett.*, *27*(4), 505–508.

Zhao, L., and L. Fisk (2010), Comparison of two solar minima: Narrower streamer stalk region and conserved open magnetic flux in the region outside of streamer stalks, in *SOHO-23: Understanding a Peculiar Solar Minimum, Astronomical Society of the Pacific Conference Series*, vol. 428, edited by S. R. Cranmer, J. T. Hoeksema, and J. L. Kohl, pp. 229–236, Astronomical Society of the Pacific, San Francisco, California.

Zhao, L., T. H. Zurbuchen, and L. A. Fisk (2009), Global distribution of the solar wind during solar cycle 23: ACE observations, *Geophys. Res. Lett.*, *36*, L14104, doi:10.1029/2009GL039181.